

# Controlling the Potential of Affordable Quasi-Solid Composite Gel Polymer Electrolytes for High-Voltage Lithium-Ion Batteries

Govind Kumar Mishra,<sup>[a]</sup> Manoj Gautam,<sup>[a]</sup> K. Bhawana,<sup>[a]</sup> Manisha Patro,<sup>[a]</sup> Shishir Kumar Singh,<sup>[a]</sup> and Sagar Mitra<sup>\*[a]</sup>

This study focuses on the development of a composite gel polymer electrolyte membrane (CGPEM) as a solution to address safety concerns arising from the reactivity of lithium metal and the formation of dendrites. The CGPEM integrates a solid polymer matrix, solid-electrolyte LSiPS ( $\text{Li}_{10}\text{SiP}_2\text{S}_{12}$ ), with a plasticizer that counteracting the performance decline caused by sulfide solid electrolyte (SSE) interactions with the cathode. Poly ethylene oxide (PEO) emerges as a promising polymer matrix due to its flexibility, cost-effectiveness, eco-friendliness, solvability for Li-salt, mechanical processing adaptability, adhesive strength, and ionic conductivity. Conductivity and processability of CGPEM were optimized through meticulous adjustment of

liquid plasticizer concentration. The CGPEM's chemical and electrochemical stability were systematically investigated using *in-situ* electrochemical impedance spectroscopy (EIS) and distribution of relaxation times (DRTs). A lithium metal battery is constructed against a high voltage cathode and newly developed CGPEM. Impressively, the cell exhibited outstanding performance, maintaining a discharge capacity of around 146.22 mAh/g after 200 cycles, retaining 86.38% of its initial capacity. The formation of a LiF-rich interface layer near the lithium surface, a vital element in curbing CGPE degradation and dendritic growth, resulted in enhanced overall cell performance.

## Introduction

Lithium (Li) metal has been extensively studied as an excellent anode material due to favorable electrochemical properties such as low reduction potential ( $-3.04$  V vs. the standard hydrogen electrode) and large specific capacity (3860 mAh/g).<sup>[1,2]</sup> The use of Li metal has opened the door to high-energy-density batteries, potentially reaching approximately 1100 Wh/L when coupled with high-capacity cathodes.<sup>[2]</sup> Nonetheless, safety concerns have arisen due to the inherent reactivity of Li metal and the formation of dendritic structures during cycling.<sup>[3–5]</sup> These needle-like Li dendrites, arising from uneven Li deposition, degrades battery efficiency and durability. Additionally, the use of flammable organic solvents in conventional liquid electrolytes<sup>[6]</sup> poses considerable safety risks when combined with Li anodes. In response to these challenges, research endeavors are shifting towards developing safer alternatives to liquid electrolytes, with a focus on solid-state batteries (SSBs).<sup>[7–9]</sup>

To mitigate the limitations linked with liquid electrolytes and enhance the security of Li metal anodes, pure solid electrolytes (SEs) have emerged as a promising solution.

Currently, the highest  $\text{Li}^+$  ionic conductivity of an inorganic solid electrolyte (ISE) at room temperature is around 12 mS/cm<sup>[5,10]</sup> however the high  $\text{Li}^+$  conductive ISEs have not been able to deliver satisfactory battery performance. Integrating SEs into battery architectures introduces its own array of challenges. The interaction between the electrode material and the SE can result in poor interface contact, impeding reaction kinetics etc. Furthermore, concerns persist regarding Li dendrite formation, as well as the chemically and electrochemically stability of the SE at both interfaces. Instability at the interface can give rise to the formation of passivation layers, hampering the transport of Li ions and fostering dendrite initiation. Over the course of cycling, stress accumulation at the interface can lead to fractures within the SE, creating conduits for dendrite propagation and causing short-circuits. Moreover, instability at the interface between the SE and cathode active materials (CAMs) can hinder the transfer of ions and electrons in composite cathodes, impacting overall battery performance. To address the limitations of pure solid electrolytes, the field has turned its attention to solid polymer electrolytes (SPEs).<sup>[11–13]</sup> These composites amalgamate the strengths of solid electrolytes with the flexibility and processability of polymers, yielding improved mechanical resilience, enhanced interfacial adherence, and improved ion conductivity. Gel polymer electrolytes (GPEs), integrating a plasticizer within a solid polymer matrix, have emerged as a tactic to surmount issues such as inadequate interfacial contact and insufficient ionic conductivity at room temperature.

Although the addition of a liquid component may at first seem to compromise safety, the plasticizer is contained

[a] G. Kumar Mishra, M. Gautam, K. Bhawana, M. Patro, S. Kumar Singh, S. Mitra  
Electrochemical Energy Laboratory, Department of Energy Science and Engineering, Indian Institute of Technology Bombay, Mumbai 400076 India  
E-mail: sagar.mittra@iitb.ac.in

 Supporting information for this article is available on the WWW under <https://doi.org/10.1002/batt.202300607>

inside the polymer matrix, results in far safer system than typical liquid systems. Additionally, compared to traditional SPEs, GPEs have shown significantly increased ionic conductivity at low temperatures, leading to higher cell performance. An appropriate balance of low cost, better electrochemical stability, and high mechanical strength is used to choose the polymer matrix. Several types of polymers have been considered for use in this application, including poly-vinylidene fluoride-co-hexafluoropropylene (PVDF-HFP), poly-methyl methacrylate (PMMA), poly-acrylonitrile (PAN), and poly-ethylene oxide (PEO). Out of all of these, PEO has received the most attention and is the most suitable polymer matrix due to its exceptional properties, such as high flexibility, low cost, eco-friendliness, strong solvability for Li-salt, superior mechanical processing, good adhesive quality, and high ionic conductivity.<sup>[2,5,17,6,10-16]</sup>

The composition of the plasticizers has a vital role on the performance of the electrolyte. It is because of the plasticizers that the GPE is able to obtain ionic conductivity levels that are equivalent to those of liquid electrolytes, with values as high as  $10^{-3}$  S/cm at ambient temperature. Ionic liquids (ILs) and the low molecular weight organic solvents are currently the two primary categories of plasticizers used, while ILs being used more frequently for fabrication of GPEs.<sup>[13,18-21]</sup> However, organic solvents are having certain disadvantages such as low molecular weight and high volatility, and tend to lose solvent with time, which reduces  $\text{Li}^+$  conductivity. In order to offset this effect, a large amount of plasticizer must be added. Unfortunately, this compromises the mechanical qualities of the GPE and raises the risk of flammability, which compromises its safety. Although ILs have major safety benefits including nonvolatility and low flammability, their application is constrained by the unacceptably high production costs linked to industrial scaling. In order to alleviate the safety issues with the GPEs-based on organic solvent, it is vital to look for a low-cost, chemically stable, and non-volatile plasticizers. In this sense, tetra(ethylene glycol dimethyl ether) (TEGDME) is a promising option. Since TEGDME is non-flammable and possesses a Li ionic conductivity of  $10^{-3}$  S/cm at normal temperature, it has been employed as an electrolyte for LIBs.<sup>[22]</sup> In PEO-TEGDME composites, it is thought that TEGDME can also increase the fraction of amorphous PEO phase and decrease PEO crystallisation, which contributes to the rapid Li-ion transport.

In this work, the synthesis and optimization of a composite gel polymer electrolyte membrane (CGPEM)-based on PEO,  $\text{Li}_{10}\text{SiP}_2\text{S}_{12}$  (LSiPS) as a ceramic active filler, and LiTFSI in tetra(ethylene glycol dimethyl ether) (TEGDME) as a liquid plasticizer, was carried out. The LSiPS solid electrolyte belong to the family of LGPS ( $\text{Li}_{10}\text{GeP}_2\text{S}_{12}$ ) superionic Li-ion conductor. LSiPS has tetragonal unit cell and belong to P42/nmc space group.4d, 4c and 16 h are the Wycoff sites for the Li atom in the crystal. The Li-ion conductivity of LSiPS is of the order mS/cm and LSiPS is cost affordable compared to LGPS, therefore the use of LSiPS to develop CGPE is economically viable.<sup>[23]</sup> By integrating the benefits of LSiPS and PEO, the aim is to craft a CGPEM with elevated mechanical attributes

and enhanced the lithium-ion transport characteristics. Key parameters such as lithium transference number, stability window, and chemical/electrochemical stability of the CGPEM will be determined through an exhaustive suite of electrochemical assessments, encompassing chronoamperometry, linear sweep voltammetry, and electrochemical impedance spectroscopy (EIS). The assembly of Li/CGPE/LCMO ( $\text{Li}_2\text{CoMn}_3\text{O}_8$ ) @LCO ( $\text{LiCoO}_2$ ) cells will be undertaken to evaluate the electrochemical efficacy of the CGPEM. The cell had a discharge capacity of  $\sim 169.27$  mAh/g with 93.76% of initial Coulombic efficiency. The cell performed excellently up to 200 cycles with capacity retention of  $\sim 86.38\%$  (discharge capacity of  $\sim 146.22$  mAh/g). The post-mortem analysis of CGPEM and Li metal suggest the formation of interface layer which is mainly dominated by LiF compound near the lithium metal surface. This LiF layer formation is essential for better performance of the cell as it inhibit further decomposition of CGPEM and dendrite formation at Li metal surface.

In summation, this investigation attempts to contribute to the advancement of CGPEs as a solution to the challenges posed by conventional liquid electrolytes and pure solid electrolytes. By tackling the constraints of prevailing materials and configurations, the intention is to pave the way for safer and more efficient lithium-based energy storage systems.

## Results and Discussion

### CGPEM properties study

The primary purpose of the study is to fabricate CGPEM, suitable for application in dendrite-free LMBs. The CGPEMs is composed of a sulfide-based ceramic electrolyte (LSiPS), a liquid plasticizer (1 M LiTFSI in TEGDME), and a polymer (PEO). Polymer electrolyte PEO is selected due to its compatibility with dissolving Li salts and its advantageous mechanical processability. Despite the impressive Li-ion conductivity and cost-effectiveness of LSiPS electrolyte, its utility has been limited by its tendency to react unfavourably with lithium metal anodes, resulting in instability. To mitigate this issue, the non-flammable and highly conductive properties of TEGDME are utilised, making it an ideal liquid plasticizer candidate. Therefore, CGPEM is synthesized through the integration of PEO/LSiPS and TEGDME, serving as an exemplary representation of an advanced GPE. The further objective of this research paper is to gain insights into the interfacial stability of as developed thin CGPEs in SSBs. This understanding is crucial for the rational design of interfaces, with the ultimate aim of enhancing the performance of dendrite-free LMB. The CGPEM films are fabricated using the solution casting method. The schematic representation of the synthesis process is illustrated in Figure 1(a). In the initial phase, PEO solution (Sigma-Aldrich, Mw = 400,000) in anhydrous acetonitrile was meticulously mixed until a transparent solution was achieved. Subsequently, a precise quantity of LSiPS SSE was mixed to it. Moving to the subsequent stage, a

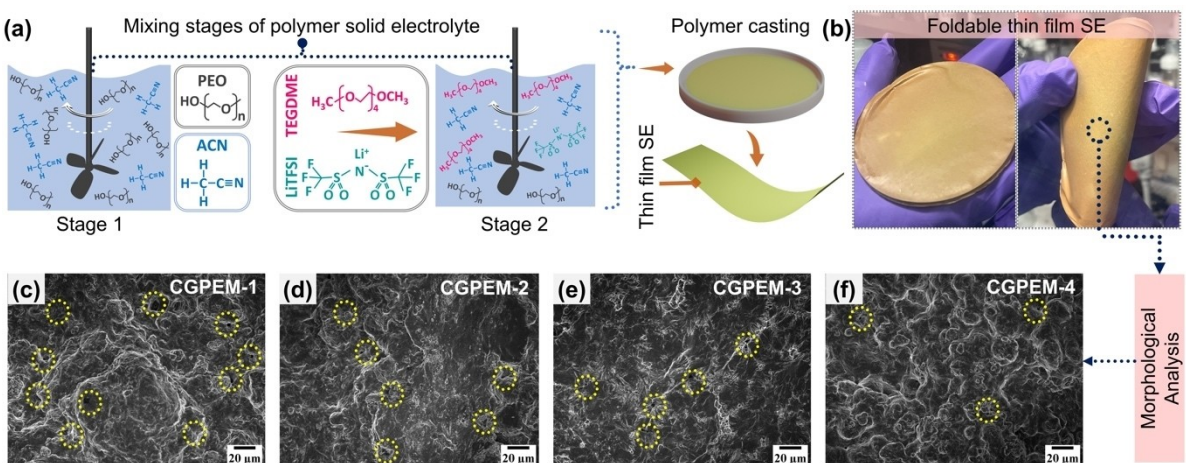


**Figure 1.** Schematics and surface morphology of CGPEM. (a) Different synthesis stages of CGPEM. (b) Digital images of synthesized CGPEM, SEM images for (c) CGPEM-1, (d) CGPEM-2, (e) CGPEM-3, and (f) CGPEM-4 compositions.

suitable amount of a mixture containing 1 M LiTFSI in TEGDME (a liquid plasticizer) was incorporated into the aforementioned solution. For the investigation conducted in this study, four distinct compositions of CGPE membranes were prepared, designated as CGPEM-1, CGPEM-2, CGPEM-3, and CGPEM-4. The weight percentage of LSIPS SSE material was consistently maintained at 50 wt.% throughout all prepared compositions. The proportions of PEO (wt. %) in CGPEM-1, CGPEM-2, CGPEM-3, and CGPEM-4 were 50, 40, 30, and 20, respectively, while the corresponding amounts of liquid plasticizer (wt. %) were 0, 10, 20, and 30, respectively.

The obtained paste was cast on the glass petri dish inside the glovebox ( $O_2$  and  $H_2O$  controlled environment) in the final step of the fabrication of the CGPE membrane. The films were subsequently allowed to undergo controlled solvent evaporation within the glovebox. For all samples, flexible, and self-supporting CGPE membrane were successfully produced. It can be noted that CGPE membranes containing less than 20 wt.% of PEO were excluded from analysis due to insufficient mechanical strength and film-forming characteristics. The comprehensive mechanical characterization of our samples is presented through a detailed stress-strain analysis, illustrated in Figure S1. To provide a succinct overview of the key findings, Table S1 encapsulates the yield strength (in MPa) and breaking strain (in %). Notably, the unplasticized CGPEM-1 sample exhibits the highest yield strength, highlighting its mechanical robustness.

Remarkably, as we delve into the impact of plasticizer concentration (or diminishing PEO concentration), a discernible trend emerges. The yield strength experiences a systematic decrease, aligning with the escalating plasticizer concentration. This trend emphasizes the crucial role of PEO concentration in influencing material strength. Notably, a pivotal observation arises beyond a critical PEO concentration threshold of 20 wt.%, where the formation of a free-standing film is impeded. This distinctive threshold marks a transition point, beyond which the structural integrity and mechanical properties of the material undergo a notable

shift. These findings contribute valuable insights into the intricate interplay between PEO concentration and mechanical behavior of CGPEM. The physical appearance of the synthesized CGPE film is depicted in Figure 1(b). The obtained film showed a flexible and self-supporting nature with a thickness ranging between 100  $\mu m$  to 200  $\mu m$ . The thickness of the film can be controlled by the simple adjustment in precursor solution, concentration or volume. The surface morphologies of the synthesized CGPEM films were examined using field emission scanning electron microscopy (FESEM), and the results are presented in Figure 1(c-f) for CGPEM-1, CGPEM-2, CGPEM-3, and CGPEM-4 samples, respectively. The SEM micrographs revealed a homogenous dispersion of ceramic LSIPS SSE powders within the polymer matrix. Notably, an increase in the amount of liquid plasticizer from 0 to 30 wt.% across CGPEM-1 to CGPEM-4 samples corresponded with a reduction in the number of pores, as indicated in Figure 1(c-f). This phenomenon can be attributed to enhanced lithium-ion percolation for the CGPEM-4 sample.

In order to determine the ionic conductivity of the as prepared CGPEMs, a broad-band dielectric spectroscopy (BDS) experiment was carried out using a sinusoidal AC wave with 50 mV of amplitude in the frequency range of 10 MHz to 1 Hz. For this experiment, conducting carbon-coated Al foil was added on both sides of the CGPEM which serves as a lithium-ion blocking electrode when measuring impedance. The obtained impedance spectra for CGPEM-1, CGPEM-2, CGPEM-3, and CGPEM-4 samples are shown in Figure 2(a-d) respectively. The ionic conductivity was calculated using the formula  $\sigma_{Li^+} = \frac{t}{R_A}$ , where  $\sigma_{Li^+}$  is the lithium-ion conductivity, t is the CGPE thickness, R is the total resistance and A is area.

The lithium-ion ionic conductivity of CGPEM-1, CGPEM-2, CGPEM-3, and CGPEM-4 samples are  $6.68 \times 10^{-7}$  S/cm,  $1.27 \times 10^{-6}$  S/cm,  $3.32 \times 10^{-4}$  S/cm, and  $7.53 \times 10^{-4}$  S/cm respectively at RT condition. In Nyquist plot, the difference between the tail portions for the CGPEM-3 and CGPEM-4 samples are quite pronounced and significant compared to

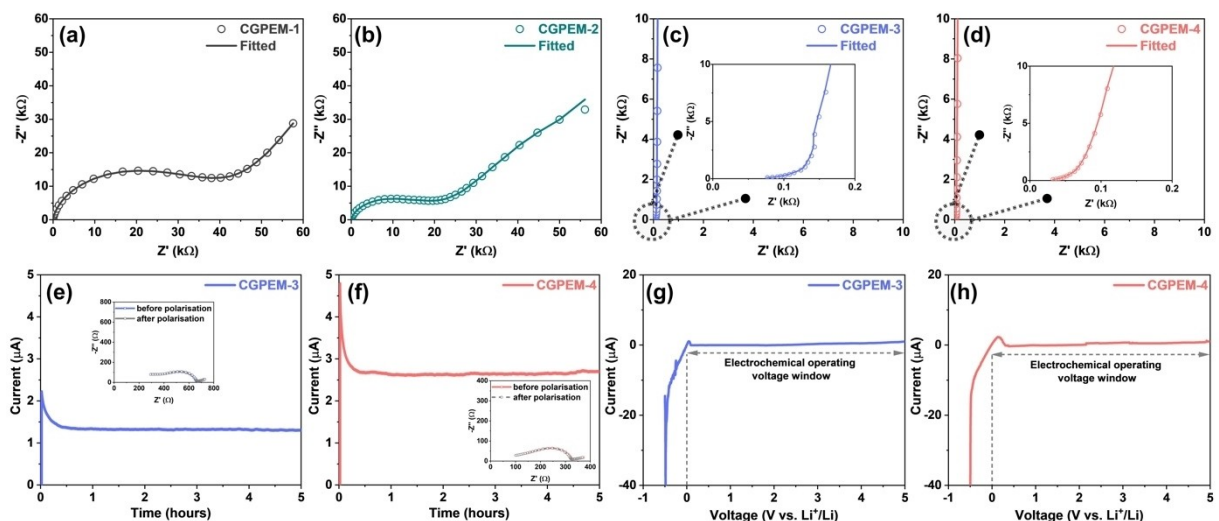


**Figure 2.** Ionic Conductivity measurements for synthesized CGPEM (a) CGPEM-1, (b) CGPEM-2, (c) CGPEM-3, and (d) CGPEM-4. Lithium-ion transference number estimation for (e) CGPEM-3, and (f) CGPEM-4 films. Linear sweep voltammetry (LSV) for (g) CGPEM-3 and, (h) CGPEM-4.

the CGPEM-1 and CGPEM-2 samples. Specifically, in the CGPEM-1 and CGPEM-2 samples, the tail portion exhibits a distinct 45° inclination, whereas in the CGPEM-3 and CGPEM-4 samples, this tail portion extends perpendicularly to real ( $Z'$ ) axis. The clarity in dataset is readily decipherable through the application of the conventional Debye circuit, under the assumptions that the solid electrolyte phase exhibits negligible electronic conductivity and the lithium ions are effectively obstructed at the electrolyte/electrode interfaces. The conventional Debye circuit is composed of a series resistance alongside an interface capacitance, denoted as  $C_{int}$ , coupled with a parallel combination of the geometrical capacitance of the electrolyte, designated as  $C_{geom}$ . This unique characteristic of the tail portion strongly implies an elevated ionic conductivity within the sample, indicative of a predominantly pure ionic conductor nature. However, in the case of the CGPEM-3 and CGPEM-4 samples, a slight departure from the pure ionic conductor behavior is noticeable. This deviation is visually apparent in the inset of Figure 2(c,d), where the tail portion deviates marginally from parallel alignment with the imaginary ( $-Z''$ ) axis.

The augmented ionic conductivity observed in the CGPEM-3 and CGPEM-4 samples, when compared to the CGPEM-1 and CGPEM-2 samples, correlates directly with a heightened presence of the liquid phase and an enhanced facilitation of lithium-ion percolation within these samples. This differentiation in the tail portion's behavior provides compelling evidence for the improved electrochemical performance in the CGPEM-3 and CGPEM-4 samples, accentuated by the favorable interplay of liquid content and lithium-ion mobility. As CGPEM-3 and CGPEM-4 samples have high ionic conductivity compared to CGPEM-1 and CGPEM-2 samples; CGPEM-3 and CGPEM-4 samples were selected for further investigation. It is critical to determine the number of ions who transport charges are present in the CGPEM. Therefore, measurement of the transference number of

lithium-ion in the CGPEMs is necessary. The experiment of Chrono-Amperometry (CA) was used for Li/CGPE/Li cell to calculate the lithium-ion transference number in CGPEM-3 and CGPEM-4 samples as shown in Figure 2(e,f). It was observed that the current amplitude gradually decreases with time. The steady current values are  $I_0 = \sim 2.215 \mu\text{A}$ ,  $I_{ss} = \sim 1.310 \mu\text{A}$ , and  $I_0 = \sim 4.689 \mu\text{A}$ ,  $I_{ss} = \sim 2.699 \mu\text{A}$  for CGPEM-3 and CGPEM-4 samples during the start and steady state, respectively. The initial current was detected at  $\sim 0\text{h}$ , then a rapid activation stage with a peak current of  $\sim 2.215 \mu\text{A}$  and  $\sim 4.689 \mu\text{A}$  was observed for CGPEM-3 and CGPEM-4 samples respectively. The EIS spectra for Li/CGPE/Li cell are shown in the inset of Figure 2(e,f). The following Bruce-Vincent formula is utilized to calculate the  $t_{Li^+}$  (transference number of lithium-ion) while taking into account the influence of polarization on the electrolyte/electrode interphase:

$$t_{Li^+} = \frac{I_{ss}(\Delta V - I_0 R_0)}{I_0(\Delta V - I_{ss} R_{ss})}$$

Where,  $\Delta V$  is the applied voltage,  $I_0$  and  $I_{ss}$ , are initial and stationary state currents, respectively,  $R_0$  and  $R_{ss}$ , are initial and steady state interphase resistance respectively. Using the above technique, the determined lithium-ion transference number is  $\sim 0.55$  and  $\sim 0.53$  for CGPEM-3 and CGPEM-4 samples respectively. The  $Li^+$  transference number of the CGPEM-3 and CGPEM-4 samples is significantly higher than that of typical polymer solid electrolytes, such as PEO-based polymer solid electrolytes, which have a  $Li^+$  transference number of only about 0.2.<sup>[24]</sup> The higher  $Li^+$  transference number was found in the CGPEM-3 and CGPEM-4 samples due to the comparatively weaker coordination of  $Li^+$  with the polymer chains. This contrasts with the robust  $Li^+$  coordination found in typical polymer solid electrolytes. Notably, this weaker coordination within the CGPEM-3 and CGPEM-4 samples serves as a catalyst for increased  $Li^+$  ion mobility.

This provides a marked enhancement in transference numbers, highlighting a better performance for these samples.

The viability of synthesized CGPEMs was assessed by studying its electrochemical voltage window for cell application. To determine the electrochemical stability window of the synthesized CGPEMs a linear sweep voltammogram (LSV) experiment was carried out for the cell with configuration of Li/CGPEM/SS at a scan rate of 50  $\mu$ V/s in the voltage range of -0.5 V to 5 V vs. Li/Li<sup>+</sup> as shown in Figure 2(g,h). For both samples, anodic and cathodic currents for lithium dissolution and lithium deposition were detected at around 0 V, respectively. It can be concluded that synthesized CGPE is stable up to 5 V and suitable with high voltage cathode because no significant currents resulting from the CGPEs failure were seen in the scanned voltage range.

The activation energy for both samples was calculated by measuring the ionic conductivity of the CGPEM-3 and

CGPEM-4 samples between 20 °C and 60 °C, at 5 °C intervals. The Arrhenius plot and their respective EIS spectra for CGPEM-3 and CGPEM-4 samples are shown in Figure 3(a,b). The temperature-dependent lithium-ion conductivity for CGPEM-3 and CGPEM-4 was linearly fitted using origin software. It was found that the average activation energies for both samples is comparable. It was determined that the activation energy for CGPEM-3 and CGPEM-4 samples are around 0.145 eV and 0.155 eV respectively.

To function CGPEMs properly in lithium-metal batteries, stability against lithium metal is essential. Therefore, CGPEMs were sandwiched between two Li-metal foils to form symmetric Li/CGPEM/Li cells in a 2032 coin-cell setup. The symmetric cell is cycled at a current density of 0.05 mA/cm<sup>2</sup> with capacity of 0.05 mAh/cm<sup>2</sup> for both the sample CGPEM-3 and CGPEM-4 at RT and shown in Figure 3(c). The CGPEM-3 sample show higher polarization voltage ~70 mV compared

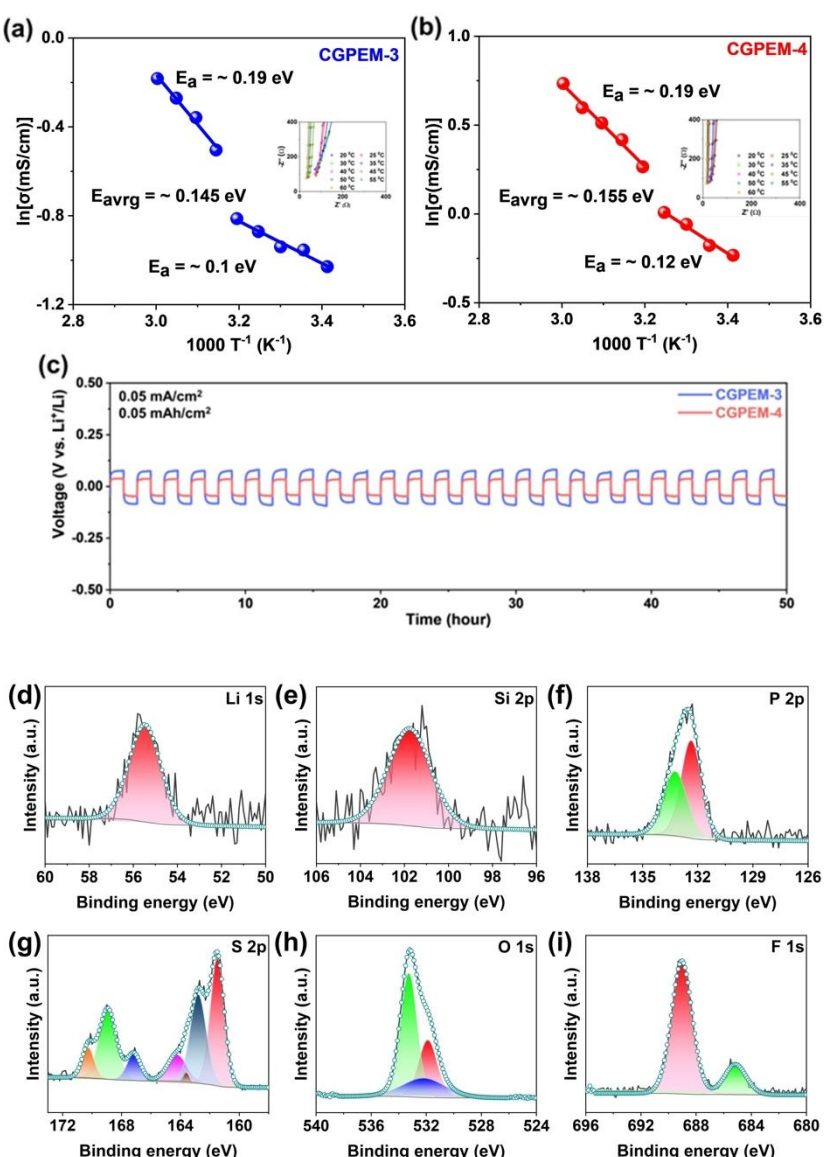


**Figure 3.** Activation energy calculation for (a) CGPEM-3. (b) CGPEM-4. (c) symmetric cell performance for CGPEM-3, and CGPEM-4. XPS analysis of CGPEM-4 (d) Li 1s (e) Si 2p (f) P 2p (g) S 2p (h) O 1s (i) F 1s.

to CGPEM-4 sample ( $\sim 35$  mV). The reason behind the less polarization voltage of CGPEM-4 sample is due to its high ionic conductivity compared to CGPEM-3 sample. Based on the above conductivity and dc polarization experiment it is obvious that CGPEM-4 sample is better compared to CGPEM-3 sample. Therefore, the CGPEM-4 sample was selected for further analysis.

It is interesting to verify the oxidation state of the ceramic SE in the CGPEM by the XPS analysis for CGPEM-4 sample. The XPS spectra of CGPEM-4 sample for Li 1s, Si 2p, P 2p, S 2p, O 1s, and F 1s are shown in the Figure 3(d-i). Li, Si, and P are present in CGPEM-4 in their desired oxidation state, according to their XPS spectra. In the S 2p spectrum, the strong double peaks at 161.48 eV and 162.77 eV corresponds to  $S^{2-}$  and peak at 163.59 eV and at  $\sim 164.24$  eV correspond to P=S-Li of LSiPS structure. The peak at 167.15 eV represents the  $Li_xS_yO_z$  whereas the peak at  $\sim 168.93$  and  $\sim 170.28$  can be assigned to LiTFSI component. The peak in O 1s spectra at  $\sim 533.27$  eV depicts the features of S=O whereas the peak at  $\sim 531.88$  and  $\sim 532.15$  shows the ROLi organic component. The F 1s spectra showed two peaks, the first one represents the C-F bond features at  $\sim 689.04$  eV whereas the peak at  $\sim 685.16$  eV represent Li-F bond nature in CGPEM. The C1s spectra is shown in Figure S2. The peak at around  $\sim 292.99$  eV, 289.92 eV, 287.65 eV, 286.78 eV and 285.09 eV represent the  $CF_3$ ,  $Li_2CO_3$ , C-N, C=O, and C-O/C-C respectively. To further verify the elemental distribution in CGPEM-4 sample the FEG-SEM elemental mapping was performed as shown in Figure S3. The elemental mapping results suggest that all the element in the CGPE is uniformly distributed throughout the sample scan area. Therefore, from above material characterization discussion it can be concluded that CGPEM was successfully synthesized and all the constituents of CGPEM are well incorporated in the film structure.

### Chemical and Electrochemical stability of CGPE against Li-metal and cell performance

The chemical and electrochemical stability of CGPE was evaluated using EIS and DRT analysis. DRT is a technique that helps interpret impedance data and can differentiate between similar polarization processes. To minimize uncertainty in identifying impedance mechanisms, the polarization resistance and specific frequency of each stage were used as starting parameters for EIS data analysis. When dealing with ideal RC elements, the polarization resistance and time constant  $\tau$  are key parameters that describe each RC pair and physical process. The two Dirac peaks in the DRT can be used to extract these characteristics directly. The relationship between the relaxation frequency and the relaxation time is represented by the formula  $f = 1/(2\pi\tau)$ , which indicates how quickly the process finds equilibrium. The two major factors that characterize the polarization process are the center frequency of its corresponding peak and the shape of the peak itself, which can be determined by the specific nature of the underlying process. To determine the overall resistance

of the polarization loss, it is necessary to integrate the area under the peak across the entire frequency range it covers. The following equation relate the EIS to its corresponding DRT:

$$Z(\omega) = R_0 + Z_{pol}(\omega) = R_0 + \int_0^{\infty} \frac{\gamma(\tau)}{1+j\omega\tau} d\tau$$

Where,  $Z(\omega)$  is the EIS data,  $R_0$  is the Ohmic resistance, and  $\int_0^{\infty} \frac{\gamma(\tau)}{1+j\omega\tau} d\tau$  denote the percentage of the complete polarization  $\tau$  and  $\tau + d\tau$  of relaxation times. The following conditions are also valid during such calculations:

$$\lim_{\omega \rightarrow 0} Z(\omega) = R_0 + \int_0^{\infty} \gamma(\tau) d\tau = R_0 + R_{pol}$$

$$\int_0^{\infty} \gamma(\tau) d\tau = R_{pol}$$

In other words, the area beneath the DRT peak is equal to the total polarization resistance  $R_{pol}$ . The impedance spectra must behave convergingly when  $\omega$  approaches zero in order to meet the boundary conditions for DRT computations. Based on the above basic description of DRT, the interface evolution between Li-metal and as synthesized CGPEM was studied in symmetric cell configuration by analysis of its EIS spectra followed by DRT analysis. It is crucial to study the stability of CGPE with Li, and therefore the chemical and electrochemical stability of synthesized CGPEM against the Li-metal was also studied.

A symmetric Li/CGPE/Li cell was fabricated and subjected to time-dependent electrochemical impedance spectroscopy (TDEIS) analysis. TDEIS measurements were performed at various time intervals, including immediately after cell fabrication (0 hours), and subsequently at 1, 5, 10, 15, 20, and 24 hours. The resulting TDEIS spectra, along with their deconvoluted distribution of relaxation times (DRT) spectra, are illustrated in Figure S4(a-g). Initially, at 0 hours, the DRT spectrum exhibited six distinct peaks. Following a resting period of 1 hour, the DRT spectrum displayed seven peaks as shown in Figure S4(b). The peaks in the high-frequency range were attributed to the formation of an interface between lithium metal and CGPE. Those in the mid-frequency range were linked to charge transfer resistance, while the low-frequency peaks were indicative of diffusion processes within CGPE and lithium metal. These peaks were identified as manifestations of inter-particle resistance, double layer relaxation processes, electrode polarizations, charge transfer at the interface, and ion diffusion resistances through DRT analysis. Notably, a specific peak at  $4.8 \mu s$  can be indicated inter-particle resistance arising from electrode-electrolyte interactions. In the range of  $\sim 37 \mu s$  to  $41 \mu s$ , a peak associated with the solid electrolyte interface (SEI) was observed. This SEI layer consists of organic and inorganic

components which were produced due to the reaction between Li metal and CGPEM. Between  $\sim$ 0.6 ms and 70 ms, three peaks pointed to charge transfer resistance at both electrodes, providing insights into electron transfer kinetics. Peaks within the range of 0.8 s to 6.3 s highlighted diffusion processes within the electrodes, reflecting ion movement dynamics. A slight increase in the first DRT peak from 0 hours to 1 hour suggested the development of an interface layer between lithium metal and CGPEM. Subsequent Figure S4(b-g) demonstrated the stability of CGPE against lithium metal, as DRT peak patterns remained constant from 1 to 24 hours. The DRT peak position and polarization resistance is shown in Tables S2-S3 for TDEIS measurement (calculated by integrating the area under each curve).

For further investigation, the Li/CGPEM/Li symmetric cell underwent charge/discharge cycles at a current density of  $0.2 \text{ mA/cm}^2$  for 1 hour each, as depicted in Figure 4(a). In-situ EIS measurements were conducted after the 1<sup>st</sup>, 5<sup>th</sup>, and 10<sup>th</sup> cycles, preceded by five-minute rests. Corresponding EIS and DRT spectra before cycling were displayed in Figure 4(b). Further EIS and DRT spectra were provided for the 1<sup>st</sup>, 5<sup>th</sup>, and 10<sup>th</sup> cycles in Figure 4(c-h), each displaying seven DRT peaks. Across all cases, DRT peak positions and polarization resistances were computed and tabulated in Tables S4-S5. The initial cycle revealed the increment in impedance and first DRT peak height due to lithium metal-CGPE interaction. Subsequent cycles showed stable EIS and DRT patterns. This stabilization pointed towards the formation of an interface layer, a crucial development that enhances the stability of CGPEM against the challenging conditions imposed by the lithium metal. In essence, the systematic investigation presented here not only sheds light on the evolving nature of the Li/CGPEM interface but also highlights the transformative impact of cyclic processes on the stability and performance of the cell. These DRT findings significantly contribute to our understanding of the intricacies involved in developing stable and efficient energy storage systems based on lithium metal and CGPEM. In conclusion, the in-situ EIS measurements and DRT spectra analysis, paints a comprehensive picture of the evolving interface between lithium metal and CGPEM. The initial cycle highlighted a discernible increase in impedance and the elevation of the first DRT peak, indicating the intricate interplay between lithium metal and CGPE. However, subsequent cycles exhibited a remarkable stabilization of both EIS and DRT patterns, pointing towards the formation of an interface layer. This layer, a product of ongoing interactions, proved to be instrumental in providing stability to CGPEM against the demanding conditions imposed by lithium metal.

Considering the cumulative findings, a Li/CGPEM/Li symmetric cell was cycled with a capacity of  $0.5 \text{ mAh/cm}^2$  and current density of  $0.5 \text{ mA/cm}^2$ , as depicted in Figure 4(i). The cell demonstrated exceptional performance with consistent polarization voltage over 200 hours. The Coulombic efficiency of lithium plating and stripping is determined with a CGPEM-4 sample using a Li/Cu cell, as shown in Figure S5. Li/Cu cell plating and stripping are carried out at a current density of

$0.1 \text{ mA/cm}^2$  with a cell capacity of  $0.1 \text{ mAh/cm}^2$ . The electrochemically inactive surface film formation is caused by electrolyte decomposition and is characterized by Coulombic inefficiency. It is clear from Figure S5 that the lithium plating and stripping through CGPEM is uniform as Coulombic efficiency is  $\sim 100\%$ . To rigorously optimize the CGPEM-4 film, we subjected it to comprehensive testing in a symmetric cell configuration (Li/CGPEM-4/Li), exploring various current densities and capacities, as illustrated in Figure S6. Impressively, the film exhibited robust performance up to  $1.0 \text{ mA/cm}^2$  of current density, along with a capacity of  $1.0 \text{ mAh/cm}^2$ . However, at an increased current density of  $1.5 \text{ mA/cm}^2$ , coupled with a capacity of  $1.5 \text{ mAh/cm}^2$ , an unexpected short circuit occurred in the cell. This outcome highlights the need for further optimization, particularly in achieving higher current densities, aiming for  $3.0 \text{ mA/cm}^2$  or beyond. Addressing this challenge will be a key focus in our future research endeavors, as we strive to enhance the overall performance and reliability of the CGPEM-4 film in practical applications.

The application of CGPEM was studied with high voltage cathode. The coin-cell is constructed using Li metal as the negative electrode, CGPEM as the electrolyte, and surface-modified LCMO@LCO as the positive electrode. The cathode slurry was composed of LCMO@LCO, super P, and PVDF in NMP solvent.<sup>[25]</sup> The cell was cycled at  $0.1 \text{ C}$  and then at  $0.5 \text{ C}$  at  $25^\circ\text{C}$  operating conditions. The mass loading of cathode active material was  $3.61 \text{ mg/cm}^2$ . The voltage profile and cyclability of the cell were displayed in Figure 4(j,k). The cell exhibited a discharge capacity of approximately  $169.27 \text{ mAh/g}$  with initial Coulombic efficiency of around  $93.76\%$ . The discharge capacity was found to be  $146.22 \text{ mAh/g}$  after 200 cycles; with a capacity retention of approximately  $86.38\%$  from the first cycle. The comparison among different CGPE is give in Table S6. To dig deeper into how well the cathode works with CGPEM at high voltages, we examined it using XPS analysis, as shown in Figure S7. Looking at the Li 1s, O 1s, and F 1s spectra, it's clear that a thin layer called the cathode electrolyte interface (CEI) forms on the cathode. This CEI is made up mostly of LiF, LixPFyOz, and some organic stuff. The presence of CEI component specially, LiF ensures that the cathode performs really well at higher voltages it acts as a protective layer.

### Post Mortem Analysis

As it was discussed earlier in DRT analysis the interface between Li metal and CGPEM is consist of inorganic and organic component. The schematic of interface formation is shown in Figure 5(a). The presence of LiF has ability to suppress the electron movement towards the CGPEM and result in dendrite suppression. To further study and confirm the interface layer formation between lithium metal and CGPEM the post mortem XPS analysis of cycled CGPEM and lithium metal was carried out. The Li 1s and F 1s XPS spectra of CGPEM is shown in Figure 5(b,c). The one additional peak, compared to pristine CGPEM, in Li 1s spectra at  $\sim 55.5 \text{ eV}$

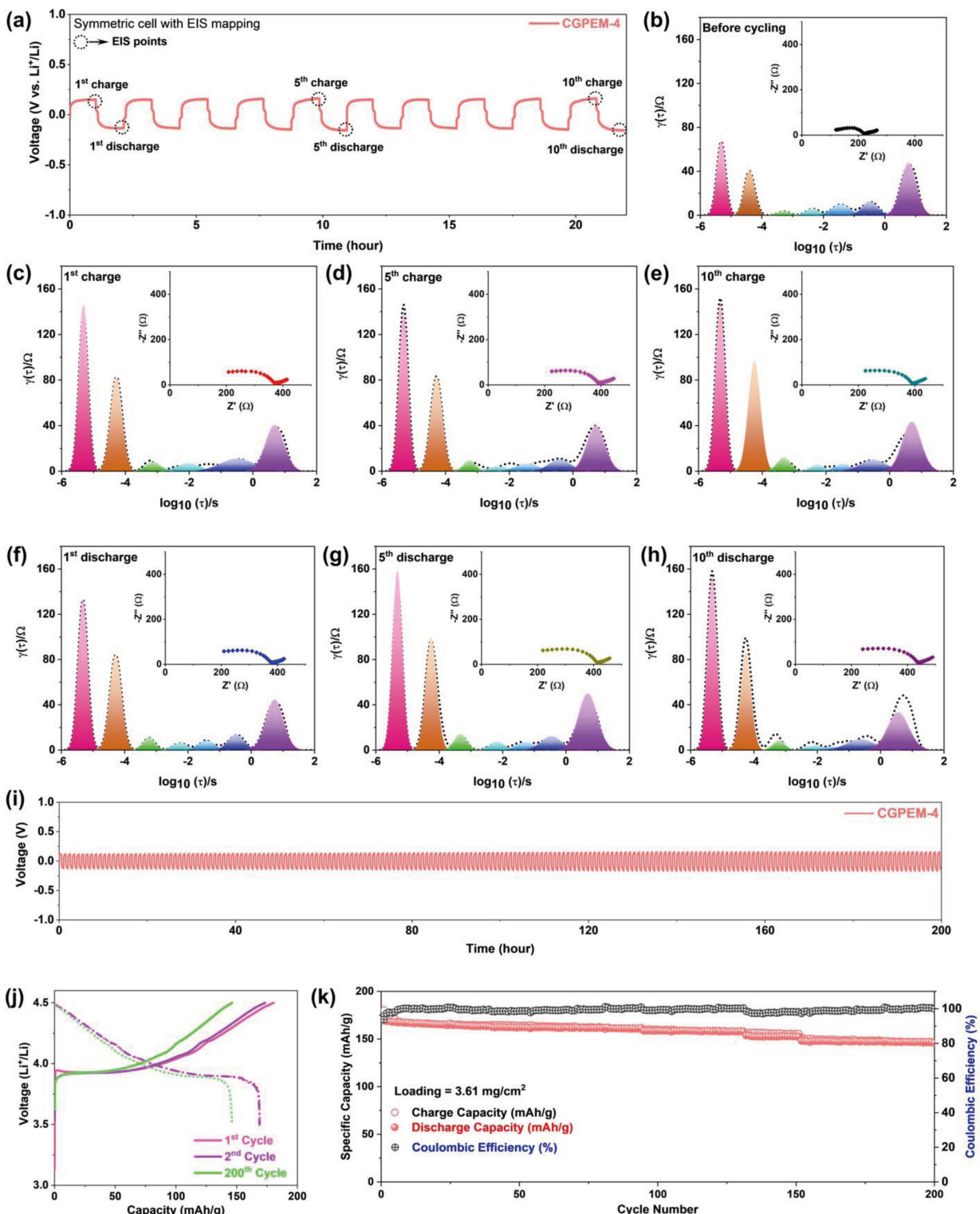


**Figure 4.** Electrochemical stability study of CGPEM and its electrochemical performance study. (a) Voltage profile for in-situ EIS study. DRT analysis for (b) Before cycling. (c) 1<sup>st</sup> charge. (d) 5<sup>th</sup> charge. (e) 10<sup>th</sup> charge. (f) 1<sup>st</sup> discharge. (g) 5<sup>th</sup> discharge. (h) 10<sup>th</sup> discharge. (i) Symmetric cell polarization study for CGPEM-4. (j) Voltage profile for Li/CGPE/LCMO coated LCO cell. (k) Cyclic stability test for Li/CGPE/LCMO coated LCO cell.

represent the formation of ROLi like organic compound at the interface between lithium metal and CGPEM. The Li 1s and F1s spectra of lithium metal after cycling is shown in Figure 5(d,e). The peak at ~55.0 eV is due to the formation of

ROLi/Li<sub>2</sub>CO<sub>3</sub> and peak at ~56.20 eV is due to the LiF. F 1s spectra of lithium metal shows two XPS peak at ~684.55 eV and ~688.74 eV and represent the LiF and C–F compounds respectively.

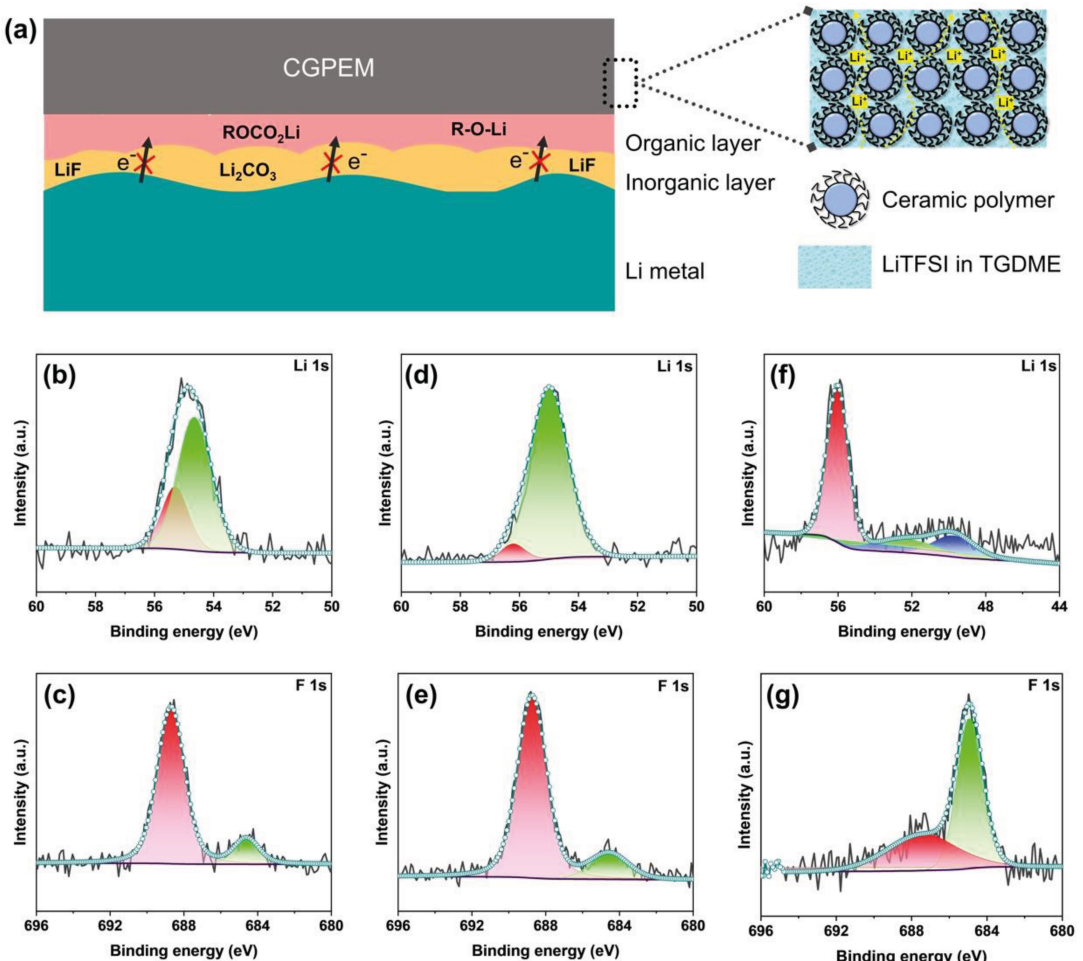


**Figure 5.** (a) Schematic representation of interface formation. Post-mortem analysis of CGPEM and Li-metal. (b) Li 1s XPS spectra of CGPEM. (c) F 1s XPS spectra of CGPEM. (d) Li 1s XPS spectra of Li-metal before etching. (e) F 1s XPS spectra of Li-metal before etching. (f) Li 1s XPS spectra of Li-metal after etching. (g) F 1s XPS spectra of Li-metal after etching.

The etching of cycled lithium metal surface was performed for 120s and XPS spectra were recorded for Li 1s and F 1s as shown in Figure 5 (f,g). The Li 1s spectra consist of three XPS peak the at ~49.90 eV, ~52.78 eV and at ~56.10 eV and these peaks corresponds to LiF, metallic lithium ( $\text{Li}^0$ ), and LiF respectively. The Li 1s spectra for lithium metal after etching shows the metallic nature of lithium and the LiF compound but there is no signature of carbonate or other organic component peak. This result suggest that the interface layer is dominated by LiF near Li surface. The previous result is further confirmed by F 1s spectra of cycled lithium metal. The F 1s spectra consist of two peaks after etching and both the peaks are located at ~684.8 eV and at ~688.0 eV and represent the LiF and C–F compound. The F 1s spectra further confirm the LiF rich layer formation between the lithium metal and CGPE. Therefore, the XPS examination and the depth profiling investigation revealed that LiF is present quite near the surface of the Li. This kind of arrangement, where a layer of LiF that is extremely dense and insulating is positioned close to the Li, is favorable because it hinders the SEI film's ability to thicken during cycling and effectively

suppresses the development of lithium dendrites. To further supplement the above conclusion SEM morphology of bare Li metal and cycled Li metal with different membranes is shown in Figure S8 and Figure S9 respectively. The SEM images showed that the surface of Li metal is uniform and no signature of Li dendrite is observed. The SEM-energy dispersive X-ray spectroscopy (EDX) mapping of the cycled Li surface with CGPEM-4 sample is shown in Figure S10. The Figure S10 clearly shows the consistent distribution of F throughout the surface. This observation suggests the formation of LiF on the Li surface. These results further confirm the effectiveness of CGPEM in preventing the formation of dendrites on the Li metal surface. The SEM image of CGPEM-4 sample is shown in Figure S11. The surface of cycled CGPEM-4 sample is dense and uniform due to the formation of SEI between Li metal and CGPEM-4.

## Conclusions

Graphite-based anodes might be replaced with metallic lithium anodes to produce SSBs with high energy densities, but using Li metal is currently risky due to its severe reactivity and dendrite growth. Although SSBs have received a lot of attention as a potential remedy, but still number of problems are remaining, including poor interface contact, insufficient dendrite prevention, low chemical and electrochemical stability of the solid electrolyte, and low ionic conductivity at room temperature. It has been suggested that solid polymer electrolytes (SPEs) are a safer option to liquid and inorganic solid electrolytes, although these technologies still require significant interfacial contact and ionic conductivity improvements. Gel polymer electrolytes (GPEs) have demonstrated potential for solving these problems by enhancing ionic conductivity by including plasticizers into the solid polymer matrix. The electrochemical performance of the electrolyte can be affected by the plasticizer used, and certain drawbacks such as the low molecular weight and high volatility of organic solvents and the high cost of ionic liquid manufacture must be addressed. Here, in this manuscript LiTFSI in TEGDME is used as a liquid plasticizer and its weight % is optimized in terms of ionic conductivity and film processability. The chemical and electrochemical stability of developed CGPE is studied through TDEIS at rest condition and *in situ* EIS measurement using the DRT analysis. The EIS and DRT analysis suggest the interface layer formation between CGPE and lithium metal which get stabilized with time. This interface layer consists of mainly LiF and confirmed by post-mortem XPS analysis. LiF layer formation is essential for better performance of the cell as it inhibit further decomposition of CGPE and dendrite formation at the lithium metal surface. The synthesized CGPE was used to construct a cell with a lithium anode and high voltage cathode. The cell had a discharge capacity of ~169.27 mAh/g along with 93.76% of initial Coulombic efficiency. The cell performance was excellent with capacity retention of ~86.38% after 200 cycles. The essence of the present findings is to provide the safe and effective strategies for the development of SSBs. This work still uses the liquid electrolyte to improve the contact at interface. Therefore, in near future our target is to improve the interface contact of electrolyte with electrodes without using any kind of liquid treatment.

## Experiments Section

### LSiPS solid electrolyte preparation

The LSiPS solid electrolyte was synthesized using the similar method as reported in our earlier publication.<sup>[23]</sup> In summary, the initial precursors, Li<sub>2</sub>S, P<sub>2</sub>S<sub>5</sub>, and SiS<sub>2</sub>, were combined inside a ball miller, undergoing mixing for a duration of 1 hour. Subsequently, the resultant powdered mixture was compressed into pellets and subjected to microwave furnace heating at 550 °C for a span of 30 minutes.

### Fabrication of PEO/LSiPS composite gel polymer electrolyte membranes (CGPEM)

The PEO/LSiPS CGPEMs were fabricated using the solution casting method. In the initial phase, PEO (Sigma-Aldrich, Mw = 400,000) was dissolved in anhydrous acetonitrile (AN) until a transparent solution was achieved. Subsequently, an appropriate quantity of LSiPS, ISE was introduced to the solution. In the subsequent step, a suitable amount of a mixture containing 1 M Lithium bis (tri fluoro methane sulfonyl) imide (LiTFSI) in Tetra ethylene glycol dimethyl ether (TEGDME) – a liquid plasticizer – was incorporated into the above solution.

Four distinct compositions of the composite gel polymer electrolyte membranes were produced: CGPEM-1, CGPEM-2, CGPEM-3, and CGPEM-4. In all four compositions, the weight percentage of LSiPS ISE remained constant at 50%. The PEO content (wt. %) in CGPEM-1, CGPEM-2, CGPEM-3, and CGPEM-4 was set at 50, 40, 30, and 20, respectively. Meanwhile, the liquid plasticizer content (wt. %) in these compositions was 0, 10, 20, and 30 for CGPEM-1, CGPEM-2, CGPEM-3, and CGPEM-4, respectively. The final step in the synthesis of the PEO/LSiPS composite gel polymer electrolyte membranes involved casting the resultant paste onto a petri dish within a glovebox. This process resulted in the formation of a self-supporting CGPEM film.

### Material characterization

Using a field emission scanning electron microscope (FEG-SEM), (Zeiss, Germany) the surface morphology of the PEO/LSiPS composite gel polymer electrolyte membrane sample was investigated. The sample was placed into the SEM chamber after being attached to a sample holder with carbon tape to study the morphology of the film. The X-ray photoelectron spectroscopy (XPS, AXIS Supra) facility<sup>[26]</sup> was used to analyze the surface chemistry of samples. The oxidation state of S, P, Si, and Li in the CGPEM was determined by XPS. The stress-strain measurement was conducted using strain-controlled rheometer (ARES G2) with cross-head speed of 40 mm/min.

### Lithium transference number and lithium ionic conductivity measurements

Within an argon-filled glove box, aluminum foil (carbon-coated) was affixed to both sides of the CGPEM film for ionic conductivity assessment. A film measuring 10 mm in diameter and approximately 220 µm in thickness was employed to gauge lithium-ion conductivity. Ionic conductivity of the film was determined through AC impedance spectra analysis using a dielectric broadband spectrometer (Novocontrol Technologies, Germany, Concept 80). The measurement spanned frequencies from 10 MHz down to 1 Hz, with an AC signal voltage magnitude of 0.05 V. For activation energy calculation, impedance spectra for ionic conductivity were captured across a temperature range of 20 °C to 60 °C, in 5 °C intervals. Electrochemical stability of CGPEM film was determined through utilizing a linear sweep voltammogram (LSV) experiment on a Li/CGPE/SS cell configuration. The experiment was conducted employing a Bio-Logic device (VMP-3 model, France) at a scan rate of 50 µV/s, covering the voltage range from -0.5 V to 5.0 V, under standard ambient conditions. The determination of lithium transference number involved a chrono-amperometry (CA) experiment on a Li/CGPE/Li cell, held at a voltage of 10 mV. To ensure test precision, EIS measurements were conducted both prior to and after the polarization scans, adhering to the approach pioneered by Bruce and Vincent. These EIS studies encompassed a frequency range of 1 MHz to

1 Hz, at a voltage of 50 mV, thereby facilitating the accurate assessment of the lithium transference number.

### Electrochemical Characterizations

To fabricate Li||Li cells, two lithium electrodes were used in a coin cell configuration, utilizing a CGPEM film to separate them. This allowed us to delve into the electrodeposition and dissolution processes under varying current densities. The experimentation was carried out at room temperature (RT) using a VMP potentiostat (Bio-Logic). Employing an AC amplitude of 10 mV, EIS measurements were carried out over a frequency spectrum spanning from 1 MHz down to 1 Hz, for Li||Li symmetric cells. Cell assembly consists of a lithium metal electrode as the negative electrode, with a CGPEM acting as a separator between the anode and cathode. Surface-modified LCO (Lithium Cobalt Oxide) material, which was synthesized following our prior publication, is used as a positive electrode.<sup>[27]</sup> The cathode was prepared by combining LCMO-coated LCO as the active material, super P as an electron-conducting medium, and PVDF as a binder. The weight ratio used was 80:10:10. The cathode slurry was thoroughly mixed before being cast onto aluminum foil and subsequently dried in a vacuum oven at 80 °C for a duration of 24 hours. The fabrication of the coin cell was taken place within a dried glovebox (MBraun, Germany) maintained under an argon atmosphere with moisture (H<sub>2</sub>O) and oxygen (O<sub>2</sub>) levels below 0.5 ppm. To ensure proper contact between CGPEM and the cathode, a small quantity (~20 µl) of liquid electrolyte (LP30) was introduced. Cyclic performance testing was conducted using an Arbin instrument, starting at a slow rate (C/10) for initial cycles and transitioning to C/2 for subsequent cycles. The voltage range tested spanned from 3.5 V to 4.5 V. The Coulombic efficiency is determined for lithium plating and stripping using a Li as a counter electrode and Cu as a working electrode with CGPEM-4 as an electrolyte. The plating areal capacity is 0.1 mA/cm<sup>2</sup> and stripping voltage is fixed to 1 V.

### Distribution of relaxation times (DRTs) analysis

The open-source script-based software MATLAB's DRT Tools was used to evaluate the impedance measurements.<sup>[28,29]</sup> A non-linear least-squares method with Tikhonov regularization was employed to fit the experimental data after the data were discretized using the Gaussian methodology. In order to fit the experimental data, the real and imaginary EIS components were employed, but inductive data was omitted. With an FWHM value of 0.5, a radial basis function (RBF) and second-order regularization derivative fitting parameters were used to successfully fit EIS data. The true impedance and DRT-produced impedance residuals were both in acceptable range using regularization parameter of 10<sup>-4</sup>. The DRT data was fitted using the Levenberg-Marquardt iteration method, and the resistance and time constant related to various polarizations were calculated. Although the base of the peak was specifically limited to zero and the number of peaks was deliberately chosen to fit peaks, other peak attributes like FWHM, area, and position were not mentioned. Several iterations were carried out until the fit converged.

### Author Contributions

The problem was conceptualized by G.K.M. and S.M. working together. G.K.M. was primarily responsible for conducting the

experiments, while S.K.S. assisted in synthesizing the composite-gel polymer film. Data analysis was carried out collaboratively by G.K.M., M.G., K.B., and M.P. All of the authors contributed significantly to writing the manuscript and approved the final version. S.M. supervised the project and provided all of the financial support.

### Acknowledgements

The authors would like to thank NCPRE, which is a project supported by MNRE India, for their assistance. G.K.M. is especially thankful for the financial support provided by the University Grant Commission (UGC) in New Delhi, India, and IRCC. K.B. and M.G. are grateful for the support of IRPHA, DST, India. The authors also express their appreciation to IRCC for XPS and strain-controlled rheometer (ARES G2). Furthermore, the authors would like to acknowledge the constant support provided by their colleagues in the ECEL lab.

### Conflict of Interests

The authors declare no conflict of interest.

### Data Availability Statement

The data that support the findings of this study are available from the corresponding author upon reasonable request.

**Keywords:** Inorganic Solid Electrolyte · High-Voltage Cathode · Solid-Polymer Electrolyte · Distribution of Relaxation Times · Transference number

- [1] J.-M. Tarascon, M. Armand, *Nature* **2001**, *414*, 359.
- [2] J. Castillo, A. Santiago, X. Judez, I. Garbayo, J. A. Coca Clemente, M. C. Morant-Miñana, A. Villaverde, J. A. González-Marcos, H. Zhang, M. Armand, C. Li, *Chem. Mater.* **2021**, *33*, 8812.
- [3] K. J. Kim, M. Balaish, M. Wadaguchi, L. Kong, J. L. M. Rupp, *Solid-State Li-Metal Batteries: Challenges and Horizons of Oxide and Sulfide Solid Electrolytes and Their Interfaces*, 2020.
- [4] M. Li, J. Lu, Z. Chen, K. Amine, *Adv. Mater.* **2018**, *30*, 1.
- [5] Y. Kato, S. Hori, T. Saito, K. Suzuki, M. Hirayama, A. Mitsui, M. Yonemura, H. Iba, R. Kanno, *Nat. Energy* **2016**, *1*, 16030.
- [6] M. Gautam, G. K. Mishra, A. Ahuja, S. Sau, M. Furquan, S. Mitra, *ACS Appl. Mater. Interfaces* **2022**, *14*, 17208.
- [7] L. Mazzaporta, A. Tsurumaki, G. Di Donato, H. Adenusi, M. A. Navarra, S. Passerini, *Energy Mater.* **2023**, *3*, 300019.
- [8] A. Le Mong, Y. Ahn, R. Puttaswamy, D. Kim, *Energy Mater.* **2023**, *3*, 300035.
- [9] M. Palluzzi, A. Tsurumaki, H. Adenusi, M. A. Navarra, S. Passerini, *Energy Mater.* **2023**, *3*, 300049.
- [10] N. Kamaya, K. Homma, Y. Yamakawa, M. Hirayama, R. Kanno, M. Yonemura, T. Kamiyama, Y. Kato, S. Hama, K. Kawamoto, A. Mitsui, *Nat. Mater.* **2011**, *10*, 682.
- [11] E. Quartarone, P. Mustarelli, *Chem. Soc. Rev.* **2011**, *40*, 2525.
- [12] D. Zhou, D. Shanmukaraj, A. Tkacheva, M. Armand, G. Wang, *Chem.* **2019**, *5*, 2326.
- [13] X. Judez, M. Martínez-Ibáñez, A. Santiago, M. Armand, H. Zhang, C. Li, *J. Power Sources* **2019**, *438*, 226985.
- [14] Q. Xiao, C. Deng, Q. Wang, Q. Zhang, Y. Yue, S. Ren, *ACS Omega* **2019**, *4*, 95.

- [15] H. Fan, C. Yang, X. Wang, L. Liu, Z. Wu, J. Luo, R. Liu, *J. Electroanal. Chem.* **2020**, *871*, 114308.
- [16] X. Wang, X. Hao, D. Cai, S. Zhang, X. Xia, J. Tu, *Chem. Eng. J.* **2020**, *382*, 122714.
- [17] Y. Xia, Y. F. Liang, D. Xie, X. L. Wang, S. Z. Zhang, X. H. Xia, C. D. Gu, J. P. Tu, *Chem. Eng. J.* **2019**, *358*, 1047.
- [18] K. M. Abraham, Z. Jiang, B. Carroll, *Chem. Mater.* **1997**, *9*, 1978.
- [19] R. He, M. Echeverri, D. Ward, Y. Zhu, T. Kyu, *J. Membr. Sci.* **2016**, *498*, 208.
- [20] G. A. Giffin, *J. Mater. Chem. A* **2016**, *4*, 13378.
- [21] M. Li, M. Kolek, J. E. Frerichs, W. Sun, X. Hou, M. R. Hansen, M. Winter, P. Bieker, *ACS Sustainable Chem. Eng.* **2021**, *9*, 11314.
- [22] J. Zheng, Y.-Y. Hu, *ACS Appl. Mater. Interfaces* **2018**, *10*, 4113.
- [23] G. K. Mishra, M. Gautam, K. Bhawana, N. Chakrabarty, S. Mitra, *ACS Appl. Mater. Interfaces* **2023**, *15*(8), 10629–10641.
- [24] K. Pożyczka, M. Marzantowicz, J. R. Dygas, F. Krok, *Electrochim. Acta* **2017**, *227*, 127.
- [25] G. K. Mishra, M. Gautam, K. Bhawana, J. Ghosh, S. Mitra, *J. Power Sources* **2023**, *580*, 233395.
- [26] K. Bhawana, A. Roy, N. Chakrabarty, M. Gautam, D. P. Dutta, S. Mitra, *Electrochim. Acta* **2022**, *425*, 140744.
- [27] G. K. Mishra, M. Gautam, S. Sau, S. Mitra, *ACS Appl. Energ. Mater.* **2021**, *4*, 14260.
- [28] K. Bhawana, M. Gautam, G. Kumar, N. Chakrabarty, S. Wajhal, D. Kumar, D. P. Dutta, S. Mitra, *Carbon* **2023**, *214*, 118319.
- [29] M. Gautam, G. Kumar, M. Furquan, K. Bhawana, D. Kumar, S. Mitra, *Chem. Eng. J.* **2023**, *472*, 144916.

Manuscript received: December 24, 2023

Revised manuscript received: January 31, 2024

Accepted manuscript online: February 2, 2024

Version of record online: February 19, 2024